Earth, Planets and Space

EXPRESS LETTER

Open Access

Distribution of *b*-value in the central and southern Ryukyu: is the low *b*-value in the rift-axis of the Okinawa Trough accurate?

Mamoru Nakamura*

Abstract

Here, I investigated whether the *b*-value in the rift-axis of the Okinawa Trough, a back-arc basin, is low. The cause of the low *b*-value in the rift-axis of the Okinawa Trough had previously been interpreted as increased stress by dyke intrusion. However, the previous study ignored the spatial variations in magnitude completeness in the Okinawa Trough. In addition, for the M4-class earthquakes that occurred in the Okinawa Trough, the values of displacement magnitudes and velocity magnitudes determined by the Japan Meteorological Agency (JMA) for the same events did not match. The previous study did not correct for these effects. Thus, I conducted these corrections and examined the spatial variation of *b*-values in the Okinawa Trough and the Ryukyu arc. The magnitude completeness was calculated using goodness-of-fit methods and the *b*-value was calculated using the maximum likelihood method. The JMA earthquake catalog from 2001 to 2019 was used for the analysis. After the corrections, the *b*-values around the rift-axis of the central and southern Okinawa Trough (0.90–0.92) were almost the same as those for the Ryukyu arc (0.83–0.84). Magnitude completeness in the Okinawa Trough varied spatially and was particularly large in the earthquake swarm area in the rift-axis of the Okinawa Trough. The steady-state magnitude completeness was 2.0 in the earthquake swarm area in the rift-axis of the Okinawa Trough. However, the magnitude completeness increased to 3.5 or higher only during the several days of occurrence of the earthquake swarms. This was caused by the short-term decrease in the ability to detect earthquakes when an earthquake swarm occurred. The finding that the *b*-values do not differ between the rift-axis of the Okinawa Trough and the Ryukyu arc indicates that stress concentration in the rift-axis of the Okinawa Trough is not a strong influence on the *b*-values. Alternatively, this might indicate that in the rift-axis of the Okinawa Trough, the distribution of low and high *b*-value regions was not detectable due to the insufficient accuracy of hypocenter determination.

Keywords: Magnitude, Earthquake swarm, *b*-value, Okinawa Trough

*Correspondence: mnaka@sci.u-ryukyu.ac.jp

Faculty of Science, University of the Ryukyus, Senbaru 1, Nishinhara-Cho, Okinawa 9030213, Japan

Graphical Abstract

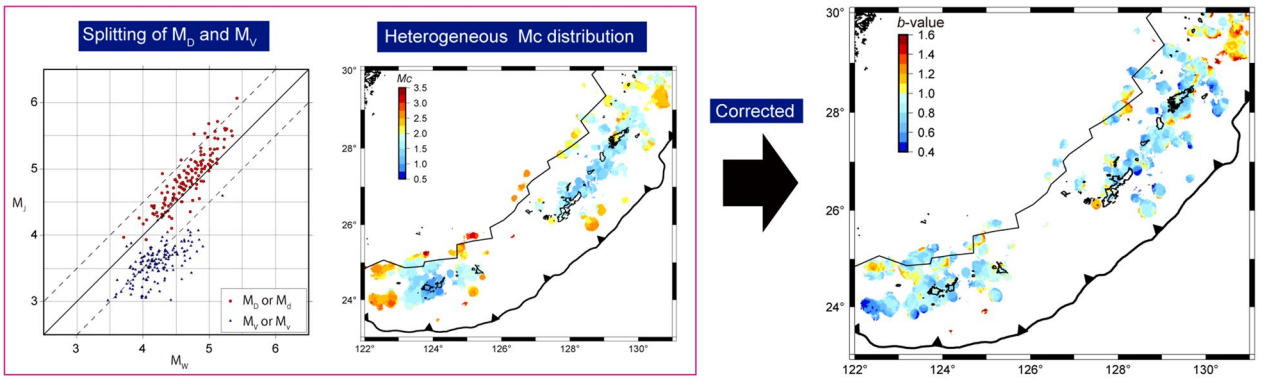

Introduction

The frequency–magnitude distribution (FMD) relates the magnitude of the earthquakes (M) and the cumulative number of earthquakes (N) (Gutenberg and Richter 1944), as shown in the following equation:

$$\log N = a - bM. \tag{1}$$

The parameters a and b are constants, and the b-value is generally close to 1 (Utsu 1971). Rock studies have reported that the b-values decrease with increasing differential stress (Scholz 1968). This result suggests that spatio-temporal changes in b-values reflect stress conditions (Wiemer and Wyss 1997; Schorlemmer and Wiemer 2005; Nanjo et al. 2012).

In the southern Okinawa Trough of southwestern Japan, low b-value (below 0.8) areas are distributed along the rift-axis of the Okinawa Trough (Arai 2021). The b-value in the Ryukyu arc is approximately 1.0–1.2, whereas the b-value in the southern Okinawa Trough is 0.5–0.9. In particular, regions with a b-value of 0.7 or less are distributed in the rift-axis of the southern Okinawa Trough. This is interpreted as being due to stress concentration due to dyke intrusion occurring in the rift-axis of the trough, resulting in a lower b-value in the earthquake swarm area (Arai 2021). Aseismic crustal deformation has been observed in the rift-axis of the southern Okinawa Trough, with possible dyke intrusion during the earthquake swarms (Tu and Heki 2017; Nakamura and Kinjo 2018). Additionally, seismic reflection surveys have found traces of dyke intrusion in the rift-axis of the southern Okinawa Trough (Arai et al. 2017).

However, the method of Arai (2021) potentially does not determine the b-value correctly in the Okinawa Trough. Clearly, it is necessary to have accurate b-values to discuss the relation between the distribution of b-values and tectonic background. To discuss the spatial variation of the b-value, the FMD must first be linear. Considering Okinawa Trough, as discussed below, the problem is that the FMD is nonlinear due to the characteristics of the Japan Meteorological Agency (JMA)'s magnitude determination scheme. Another problem is that the previous analysis uses earthquakes with smaller magnitude than the earthquake detection capacity (magnitude completeness [M_C]). However, it is possible that M_C is actually changing in time and space. Therefore, this study first provides an explanation of these two issues. After correcting for these effects, I examined b-values in the central to southern Okinawa Trough rift-axis and investigated whether the low b-values in the southern Okinawa Trough rift-axis were due to these problems.

Nonlinear FMD caused by magnitude determination scheme

If the FMD of seismicity is not linear, the accurate b-value cannot be determined. For example, when multiple earthquake swarms with different M_C are analyzed together, a nonlinear FMD is generated (Wiemer and Wyss 2000). In another case, the linearity of the FMD may not hold due to incomplete methods of magnitude determination. In 2003, the JMA revised the method of magnitude determination. Before 2003, when the displacement magnitude (Tsuboi 1954; Katsumata 1964) and velocity magnitude (Kanbayashi and Ichikawa 1977; Takeuchi 1983) were determined, the JMA set the average of both to the JMA magnitude (M_J) for the earthquake. After the change, new formulas for displacement magnitude (Katsumata 2004) and velocity magnitude (Funasaki et al. 2004) were adopted. Moreover, when displacement magnitude and velocity magnitude are determined, both are listed in the catalog, and the displacement magnitude is given priority over the JMA magnitude. The exact preference of priority for JMA magnitudes is as follows:

displacement magnitude (M_D) using three or more stations, velocity magnitude (M_V) using four or more stations, displacement magnitude (M_d) using fewer than three stations, and velocity magnitude (M_v) using fewer than four stations. The previous JMA magnitude underestimated the cumulative number of earthquakes with magnitudes around M4.0–4.5, compared to what would be expected from the FMD. This was caused by the fact that the previous JMA magnitude tended to calculate a velocity magnitude smaller than the displacement magnitude for earthquakes over M4.0 (Funasaki et al. 2004). Since 2003, the magnitude formula was thus revised to reduce the above trend, resulting in a linear FMD connecting the cumulative number curves for earthquakes over and below M4.0 (Data Analysis Section, Earthquake Prediction Information Division, Seismological and Volcanological Department, Japan Meteorological Agency 2004). As a result of the improvements, the cumulative number of earthquakes at the new JMA magnitude almost satisfied the linear FMD requirement.

However, the difference between displacement magnitude and velocity magnitude remained large in some areas even after the improvement, particularly in the Ryukyu area. In earthquakes off the northwest coast of Ishigaki Island, the displacement magnitude is approximately 0.5 greater than the velocity magnitude (Data Analysis Section, Earthquake Prediction Information Division, Seismological and Volcanological Department, Japan Meteorological Agency 2004). This effect decreases the frequency of earthquakes around M_J 4.0, using the new JMA magnitude. Notably, this was not seen in the frequency distribution of earthquakes using the previous earthquake catalog. This feature becomes evident by comparing M_J and moment magnitude (M_W) from the Full Range Seismograph Network of Japan (F-net) centroid moment tensor (CMT). The M_W 4.0–5.0 earthquake group can be separated into larger and smaller M_J, depending on whether M_D or M_V (or M_v) is employed (Fig. 1b). If M_D is adopted for the analysis, the M_J is determined to be 0.17 larger than the M_W. In contrast, if M_V is adopted, the M_J is determined to be 0.63 smaller than the M_W. This causes the counted number of M_J 4.0–4.5 earthquakes to be lower. The FMD of M_W shows no decrease in the frequency between M_J 4 and M_J 5, while the FMD of M_J shows a depression in frequency from M_J 4.0 to M_J 4.2 (Fig. 1c and d). When the M_C in M_J is around M_J 4.0, the apparent b-value calculated will be smaller, as the slope of the FMD becomes gentler around M_J 4.0–5.0.

Spatio-temporal change in *MC*

The second problem is regarding the temporal and spatial variation of M_C. Immediately after a major earthquake, many aftershocks are missed from observations when the high frequency of aftershocks exceeds the discriminating ability of the observation network (Ogata 1983; Utsu et al. 1995; Kagan 2004). For M7-class earthquakes, the M_C increased by 0.5–1.0 for 0.5–3 days immediately after the mainshock (Wiemer and Katsumata 1999). In the southern Ryukyu arc and southern Okinawa Trough, the M_C has been less than 2.0 since 2001 (Nakamura and Kinjo 2018). However, when earthquake swarms occurred in the southern Okinawa Trough, the M_C increased temporarily. Figure 2 shows the temporal variation of M_C values in the southern Okinawa Trough. Active earthquake swarms were observed off the north coast of Ishigaki Island in October 2002 and April 2013 (Fig. 2a). The M_C values in this region were approximately 2.0 before 2003 and ranged from 1.6 to 2.0 after 2003 (Fig. 2b). However, during the October 2002 earthquake swarm, the M_C increased temporarily to 3.8 (Fig. 2b). Similarly, during the 2013 earthquake swarm, the M_C increased temporarily to 3.2 (Fig. 2b). The period of increased M_C was very short (a few days). However, most of the seismic activity in the rift-axis of the Okinawa Trough is due to short-term earthquake swarms. Alternatively, the b-value could be calculated using the smaller steady-state M_C, even though the M_C increased due to the swarm earthquakes. In this case, the FMD slope would be determined by including the magnitude range of many undetected earthquakes. This would have caused the underestimation of the b-value in the rift-axis of the Okinawa Trough. The increased M_C during earthquake swarms was also observed in other earthquake swarms in the Okinawa Trough (Additional file 2: Figure S1–S2).

Data and methods

The JMA catalog was used as the hypocenter list in the analysis. The period was January 1, 2001, to December 31, 2019; earthquakes occurring in 23.0°–30.0°N, 122.0°–131.0°E were used. Depths ranged from 0 to 40 km. Earthquakes with at least five seismic stations were used in the analysis. M_C and b-values were calculated using M_V (or M_v) from the JMA catalog to remove effects of the separation of M_J around M_W 4.0. Essentially, M_D should be used because it is closer to M_W (Fig. 1b). However, M_D can only be used for large magnitude earthquakes, so the number of earthquakes used for analysis is small, as large earthquakes are limited to

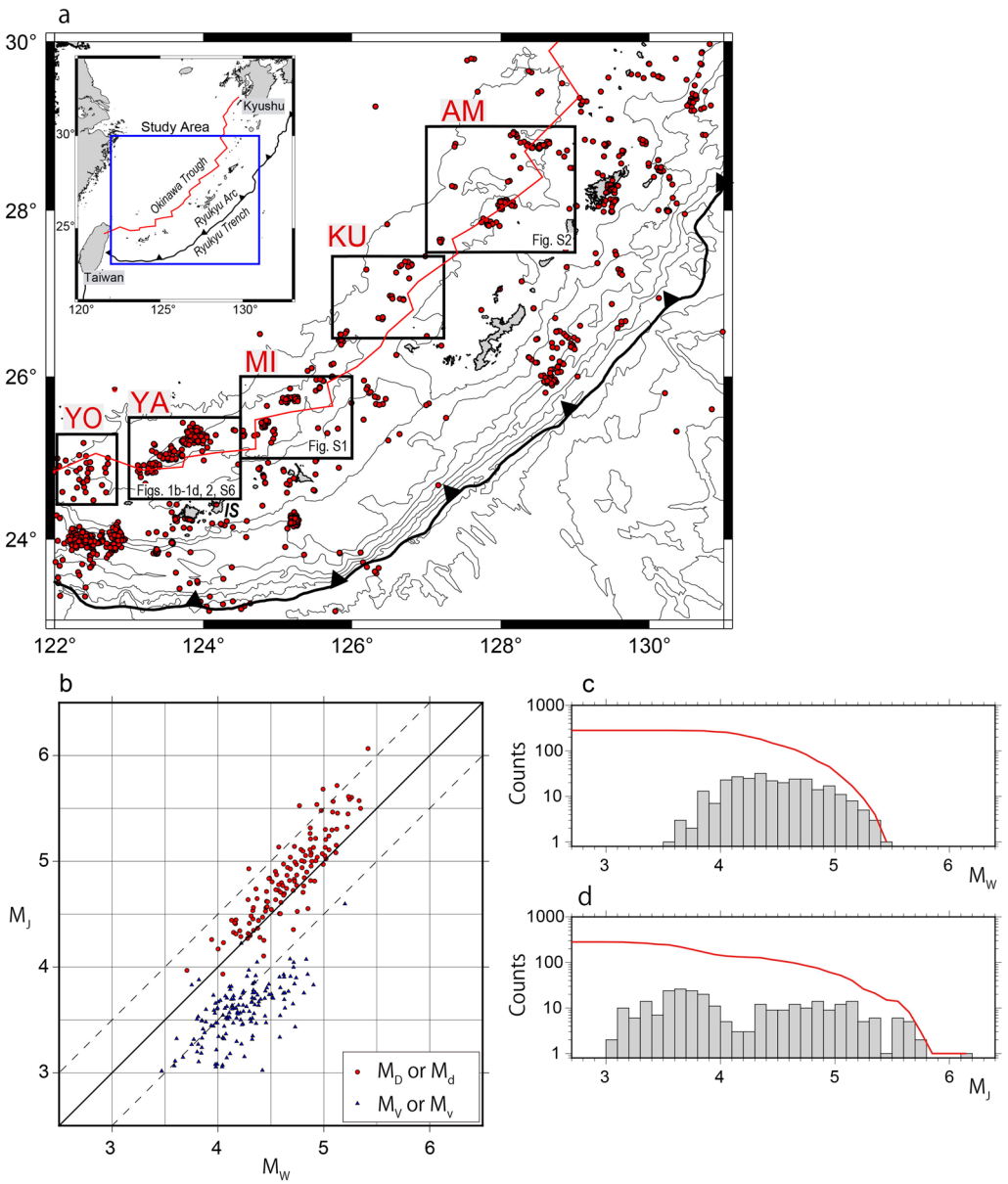

Fig. 1 Regional map and comparison of M_W and M_J (January 2001–December 2019). **a** Distribution of hypocenters in the Ryukyu (M ≥ 3.0, January 2001–December 2019). YO: Yonaguni area; YA: Yaeyama area; MI: Miyako area; KU: Kumejima area; AM: Amami area, IS: Ishigaki Island. Red circles indicate earthquakes. The contour is bathymetry from Chikasada (2020). The location of the plate boundary is from Bird (2003). The inset shows the regional tectonic map. **b** Comparison of M_W and M_J at YA. The calculation area is shown in Figurer 1a. Red circles indicate M_D or M_d, and blue triangles indicate M_V or M_v. The rectangle indicates the calculation region. To distinguish the density of the points on plot, a uniform random number between -0.05 and 0.05 was added to the magnitude value and displayed in the figure. **c** FMD of M_W. Bars show the number of earthquakes for each bin. The red line indicates the cumulative number of earthquakes. **d** The same as **c** but for M_J

a narrow area. Therefore, it is impossible to determine the spatial variation of *b*-values using M_D. Thus, the M_V was obtained for the smaller magnitude earthquakes that were used in the analysis. For large earthquakes, M_D and M_W are listed, but not M_V. In this case, the velocity magnitude at each station was calculated using the equation of Katsumata (2007) with the maximum vertical component amplitude from the arrival time catalog of JMA, and the average of these values was used as the M_V (Additional file 1: Table S1).

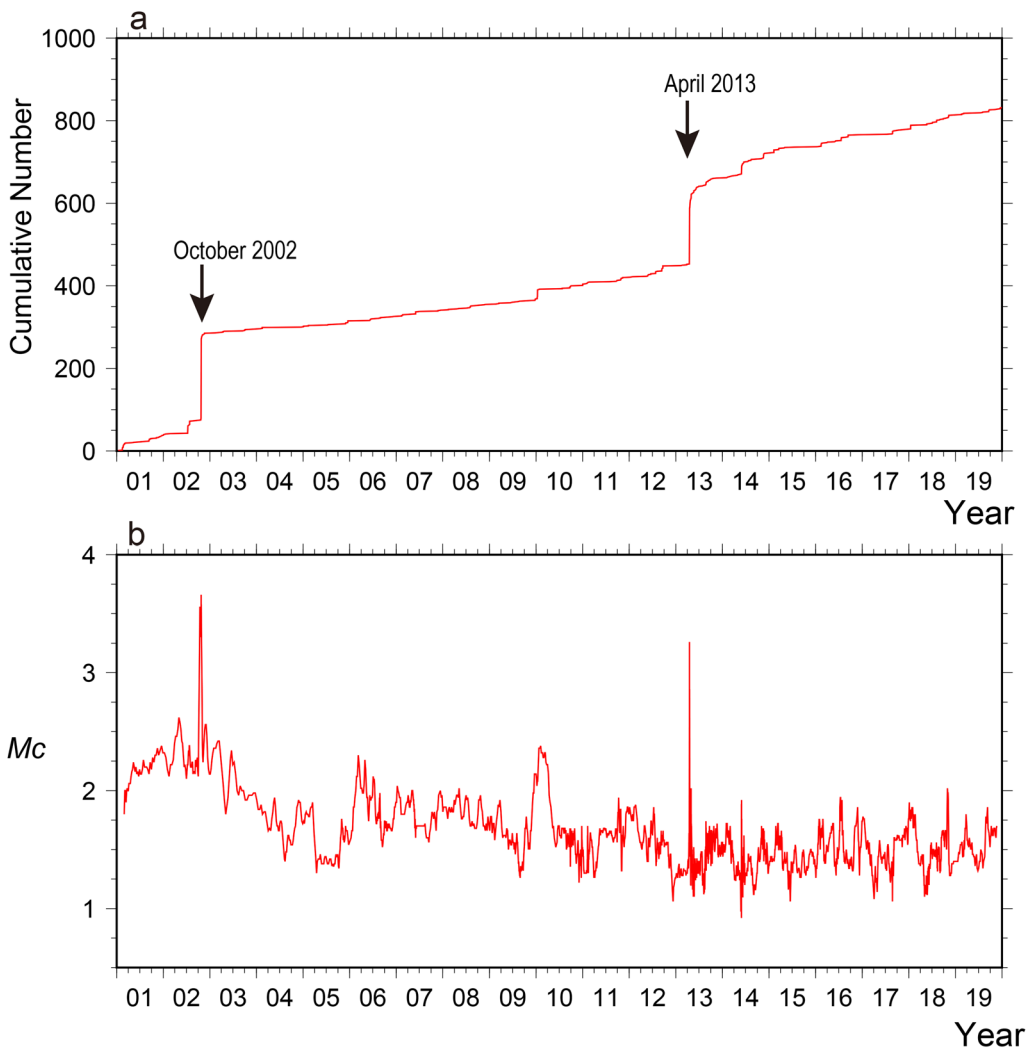

Fig. 2 Cumulative earthquake number and time variation of M_C off the northwest coast of Ishigaki Island. **a** Cumulative number of earthquakes ($M_V \geq 3.0$). The calculation area is shown at Figurer 1a. Red circles show earthquakes. Arrows show the October 2002 and April 2013 earthquake swarms. **b** Time variation of M_C. M_C was calculated using Zmap7, shifting by 5% for every 100 earthquakes on the time axis

M_C and b-values were calculated using the ZMAP version 7 software package (Wiemer 2001). The M_C was calculated using goodness-of-fit methods (Wiemer and Wyss 2000, 2002). As in Wiemer and Wyss (2002), the goodness-of-fit level was set at 90%.

The b-value was calculated using the maximum likelihood method (Aki 1965; Utsu 1965):

$$b = \frac{\log_{10} e}{M_{Mean} - M_0}, \tag{2}$$

where M_{mean} is the mean magnitude; it can also be expressed as $M_o = M_C - 0.05$ for a magnitude bin of width 0.1.

The procedure for determining M_C is as follows. First, earthquakes larger than magnitude M_i are selected, and the maximum likelihood method is used to obtain the values of a and b for FMD. Next, synthetic FMD is computed using M_i, a, and b. Next, the absolute difference, R, between the observed and synthetic FMD at each magnitude is calculated to obtain the goodness-of-fit level (Wiemer and Wyss 2000):

$$R(a, b, M_i) = 100 - \left(\frac{\sum_{M_i}^{M\max} |B_i - S_i|}{\sum_i B_i} 100 \right), \tag{3}$$

where B_i and S_i are the observed and synthetic cumulative number of earthquakes in each magnitude bin. R is calculated by increasing M_i; when there are a certain number of earthquakes above M_i, and the R reaches 90% or more, the M_i obtained above is adopted as M_C. The FMD coefficient b is adopted as the b-value. M_C and b-values were calculated when there were more than 50 earthquakes within the search radius to align conditions with those of Arai (2021).

The examples of ill-behavior and well-behavior for FMD are shown in Additional file 2: Figure S3. In the case of ill-behavior, 184 earthquakes within a radius of 10 km were counted at 25.696°N and 124.995°E in Miyako area (MI) (Additional file 2: Figure S3a). However, no M_C and b-values were determined. The nonlinear FMD is caused by the two earthquake swarms that occurred in April 2007 and October 2016; in 2007 and 2016, the M_C values in the vicinity were 3.3 and 2.8, respectively (Additional file 2: Figure S1). The combination of seismic activity with different M_C made the FMD nonlinear, making it impossible to determine the M_C and b-value under the condition of more than 50 earthquakes. Additional file 2: Figure S3b shows the well-behavior case for FMD. There were 3515 earthquakes within a radius of 10 km and 2370 earthquakes with $M_C = 1.6$ or greater. From this M_C, the b-values were calculated.

M_C and b-values were calculated at 1-km intervals within the area. Earthquakes within a radius of 10 km from each point were used in the analysis. Expanding the search radius increases the number of earthquakes included in the area, thus reducing the number of points where M_C and b-values cannot be determined. However, some areas had M_C and b-values, although earthquakes did not occur in the area. Therefore, considering the error in determining the epicenter (according to the JMA catalog, the horizontal error in the southern Okinawa Trough is within approximately 6 km), the search radius was set at 10 km.

Results

Whether M_V (or M_v) or M_J was used in the calculations, the M_C near the rift-axis of the central and southern Okinawa Trough (1.6–3.6) showed higher values than those in the Ryukyu arc (1.0–2.0) (Fig. 3b and Additional file 2: Figure S4b). Small M_C (1.4 to 2.2) was distributed in the Yaeyama area (YA) (see Fig. 1a for locations). However, the M_C was high in other earthquake swarm areas (Fig. 3b). For example, the M_C reached 3.6 on the central part of the YA (25.2°N, 124.0°E). In the MI (25.6°N, 125.0°E), the M_C ranged from 2.4 to 3.4. The M_C was approximately 2.5 in the Kumejima area (KU). The M_C was approximately 2.0 in the Amami area (AM), which was smaller than that in the central to southern Okinawa Trough. The M_C values at each location were basically almost constant during 2001–2019. However, the M_C increased during the earthquake swarm. In the MI, the M_C ranged from 2.2 to 2.8 from 2001 to 2019. However, the M_C increased to 3.3 during the 2007 earthquake swarm in the MI (Additional file 2: Figure S1). In the AM, the M_C was in the range of 2.5–3.0 until 2008. However, since 2009, the M_C has been in the range of 1.5–2.0. Furthermore, during the 2009 and 2014 earthquake swarms, the M_C briefly increased to 3.0 and 2.4, respectively (Additional file 2: Figure S2). The M_C increased with earthquake swarm activity during the other years.

The b-values were almost the same when either M_V (or M_v) or M_J was used, except for the central YA (Fig. 3a and Additional file 2: Figure S4a). The b-values from M_V ranged from 0.7 to 1.3 in the rift-axis of the Okinawa Trough; in the YA, the b-values ranged from 0.7 to 0.9. However, in the Yonaguni area (YO) (24.8°N, 122.5°E), the b-value increased to 1.1–1.3. In the central part of MI (25.6°N, 125.0°E) and western part of the YA (24.7°N, 123.2°E), the b-values were slightly higher (0.8–1.2). The b-values ranged from 0.7 to 1.1 in the KU, and from 0.8 to 1.2 in the AM.

The b-value in the central part of the YA (25.2°N, 124.0°E) depended on the magnitudes used. In the central part of YA, the value of M_C was almost the same (~3.3) for both M_V and M_J (Fig. 3a and Additional file 2: Figure S4a). However, the b-value by M_J was 0.4, while the b-value by M_V was 0.7 (Figs. 3b and S4b).

No marked differences were found between the frequency distribution of b-values along the Ryukyu arc and along the Okinawa Trough (Fig. 4). The b-values were 0.90 ± 0.16 for the southern Okinawa Trough (area a), 0.84 ± 0.13 for the southern Ryukyu arc (area c), 0.92 ± 0.18 for the central Okinawa Trough (area b), and 0.83 ± 0.17 for the central Ryukyu arc (area d). The b-values for the entirety of the box were 0.61 for the southern Okinawa Trough, 0.62 for the southern Ryukyu arc, 0.79 fort the central Okinawa Trough, and 0.69 for the central Ryukyu arc. The M_C values were 1.3–3.5 for the southern Okinawa Trough, 0.7–2.5 for the southern Ryukyu arc, 1.6–2.6 for the central Okinawa Trough, and 0.8–2.7 for the central Ryukyu arc (Additional file 2: Figure S5). The M_C values for the entirety of the box were 1.6 for the southern Okinawa Trough, 1.0 for the southern Ryukyu arc, 1.8 fort the central Okinawa Trough, and 1.4 for the central Ryukyu arc.

Discussion

Unlike the results of Arai (2021), the b-value in the rift-axis of the southern Okinawa Trough was almost the same as the b-value in the Ryukyu arc. One reason for this is that the previous study did not consider the effect

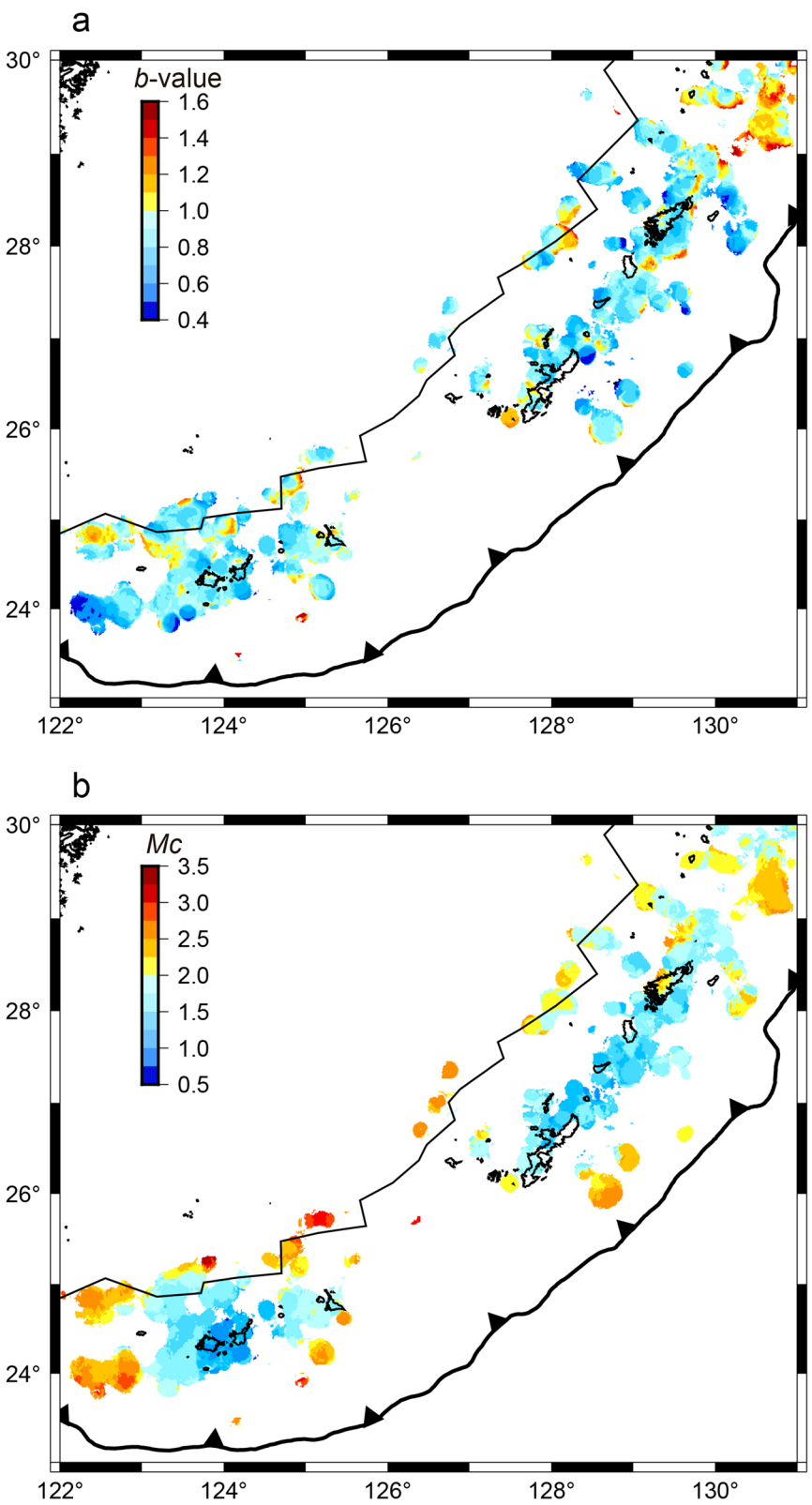

Fig. 3 Distribution of *b*-values and M_C in the south-central part of Ryukyu, determined by velocity magnitude. **a** Distribution of *b*-values. The location of the plate boundary is from Bird (2003). **b** Distribution of M_C

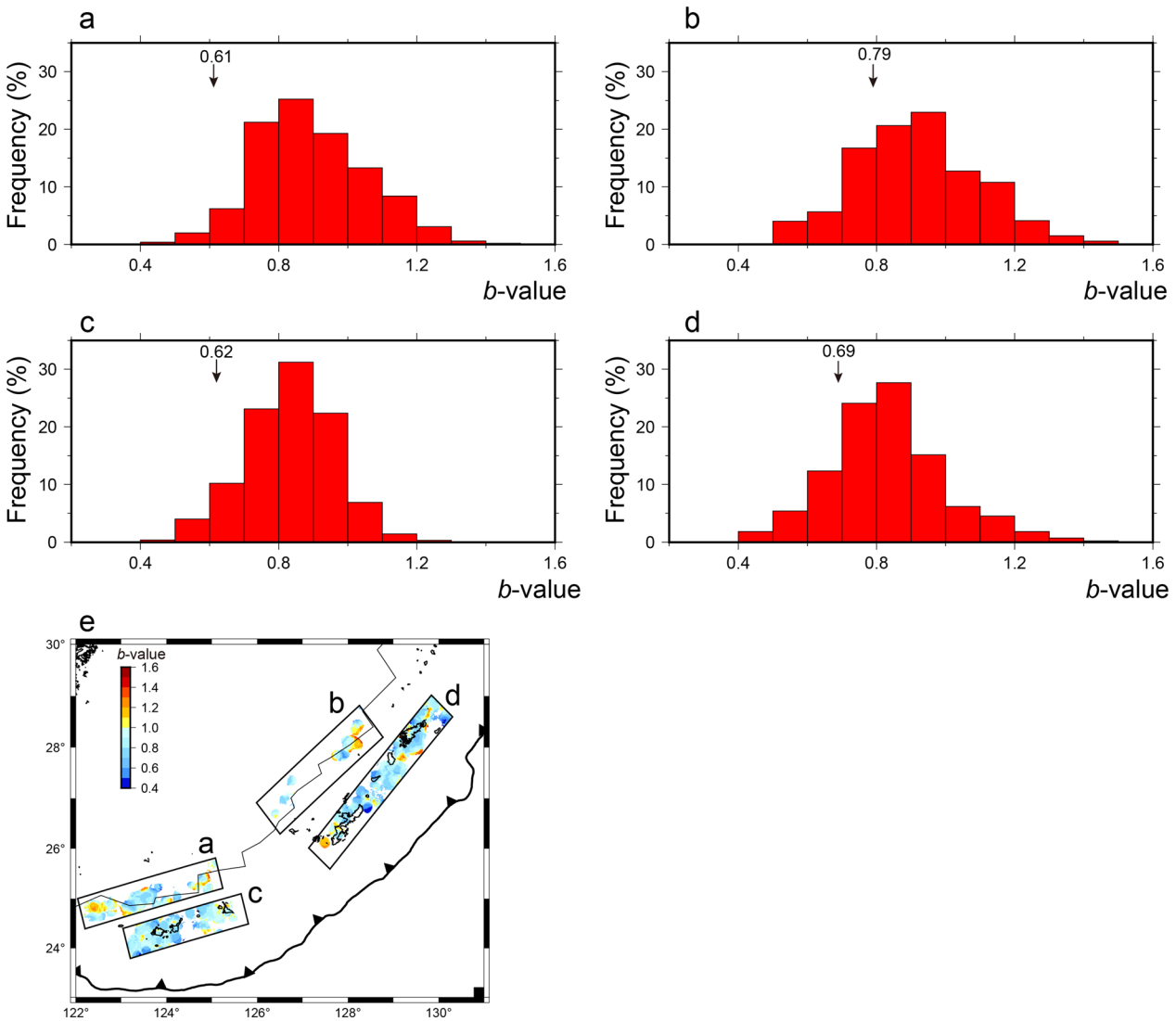

Fig. 4 Frequency distribution of *b*-values in each region. **a** Frequency distribution of *b*-values in the southern Okinawa Trough. *b*-values were calculated using M_V. The numbers with arrow show the *b*-value for the entirety of the box. **b** The same as **a** but in the central Okinawa Trough. **c** The same as **a** but in the southern Ryukyu arc. **d** The same as **a** but in the central Ryukyu arc. **e** The area of each region is shown. The *b*-values are shown in color. The location of the plate boundary is from Bird (2003)

of spatial variation in M_C. In the YA, the M_C was approximately 2.0 (Fig. 2b). However, when the earthquake swarms occurred, the M_C increased to 3.0–3.5 (Fig. 2b). If the M_C is estimated to be smaller than the actual value, the FMD slope will be calculated according to the magnitude range, including undetectable small earthquakes, resulting in an estimated *b*-value that is lower than the true one. For these reasons, the low *b*-values (< 0.6) in the YA and MI, which were observed in the previous study, were apparent values. After an appropriate M_C was used, the area of low *b*-values (below 0.8) almost disappeared (Fig. 3a). In the previous study, since the *b*-value was calculated with constant M_C across the region, without considering the temporal and spatial heterogeneity of M_C, a lower *b*-value appeared.

Another factor is the discontinuity between M_D and M_V around M4.0, which led to an apparent decrease in the number of earthquakes around M_J 4.0 and a local flattening of the FMD slope (Fig. 1d). For example, consider that the discontinuity between M_D and M_V occurs around M_J 4.0. In this case, if the M_C is sufficiently smaller than M_J 4.0, the discontinuity will have little effect on the *b*-value. However, when the M_C increases and becomes close to M_J 4.0 due to earthquake swarm activity, the estimated

b-value would be smaller. The M_D and M_V discontinuity effects do not affect the estimation of *b*-values in most areas. However, in the October 2002 earthquake swarm area in YA, the *b*-values calculated using the M_J were different from those using M_V; the very low *b*-values calculated using M_J would be due to the high M_C and splitting of M_D and M_V.

M_C is high (1.6–2.8) in both the southern and central Okinawa Trough (Additional file 2: Figures S5a and b). Contrastingly, in the Ryukyu arc, M_C is low (0.9–1.8) in both the southern and central Ryukyu arc (Additional file 2: Figure S5c and d). This indicates that the seismic network is located only in the islands; thus the detection capability is high in the vicinity of the islands, while it is low away from the islands, such as in the Okinawa Trough. The value of M_C calculated using earthquakes along the entire southern Okinawa Trough rift-axis is 1.6. However, each grid's M_C is considerably variable, ranging from 1.6 to 2.8. This variation would be caused by the low earthquake detection capability of the Okinawa Trough and the effect of a temporary increase in M_C due to earthquake swarm activity. Another notable feature of M_C in the Okinawa Trough is that the M_C for the entire region corresponds to the lower end of the M_C calculated for each grid. This indicates that even if the M_C for the whole area is sufficiently small, it would not be reasonable to use that M_C for the whole area when estimating the *b*-values for each grid in the region.

In the case of the October 2002 earthquake swarm in the YA area, the large number of earthquakes with detectable events in the seismic waveforms but not determined hypocenters was another factor that contributed to the large M_C. Indeed, there were many earthquakes in the 2002 earthquake swarm whose waveforms were recorded but whose epicenters have not been determined. When the earthquake swarm began at 6:00 Japan Standard Time (JST) on October 24, a few earthquakes below M_J 3.0 were determined, and the M_C was approximately 4.0 (Fig. 5a). F-net waveforms at station IGK (epicentral distance from the earthquake swarm area was approximately 100 km) at 7:13–7:45 JST showed several small spindle-shaped waveforms whose hypocenters were not determined by the JMA (Fig. 5b). These waveforms were similar to those of the M_J 3 class earthquakes that immediately preceded and followed. Therefore, the spindle-shaped waveforms should also correspond to earthquakes that occurred in the earthquake swarm area. For example, between 7:16 and 7:20 and between 7:35 and 7:42, the waveform at IGK showed multiple spindle-shaped waveforms (blue lines in Fig. 5b). Assuming that the hypocenters were within the earthquake swarm area, these M_v were estimated to be 2.2–2.7, based on the maximum amplitude of the spindle-shaped part (2000–6000 nm/s). This means that the earthquakes of M_v 2.2 to 2.7 were distinguishable from the noise in IGK, but their hypocenters could not be determined. In the waveform at station YNG (epicentral distance from the earthquake swarm area was approximately 140 km), the spindle-shaped waveforms corresponding to those at IGK were very difficult to detect because they were obscured in the noise. As P and S phases could not be picked up at any stations other than those near Ishigaki Island, there observations were not sufficient to determine the hypocenters.

As the magnitude increases, the number of seismic stations available to detect seismic waves increases. It is possible that the difference in the number of used seismic stations leads to a bias in the hypocenter location and affects the *b*-value. To investigate the bias between the number of seismic stations and hypocenters, I examined whether the hypocenter distribution of the same magnitude range is different with a different number of stations (Additional file 2: Figure S6). In area A, for both M2.0–3.0 and M3.0–4.0 earthquakes, epicenters with many seismic stations were concentrated in the south. In contrast, the north part of area A gathered epicenters with fewer seismic stations, i.e., smaller magnitude earthquakes tended to be distributed in the north part of the earthquake cluster. M2.0–3.0 earthquakes are distributed farther north than M3.0–4.0 earthquakes. Therefore, a high *b*-value area is generated on the northern edge of the earthquake cluster (Fig. 3a and Additional file 2: Figure S6c). In area B, for earthquakes of magnitude 2.0–3.0, epicenters with many seismic stations were distributed north of epicenters with a smaller number of seismic stations. M3.0–4.0 earthquakes are distributed north of the M2.0–3.0 earthquake cluster. Therefore, larger earthquakes were more likely to be distributed to the north and smaller earthquakes are distributed in the south, resulting in high *b*-values in the southern part of the cluster (Fig. 3a and Additional file 2: Figure S6c). The bias in the hypocenter location due to the difference in the number of seismic stations could be responsible for the anomalous *b*-values at the edges of the earthquake cluster.

The *b*-values in the central and southern Okinawa Trough (0.7 to 1.2) were within the *b*-values observed at the mid-ocean ridge (MOR). The *b*-values at Rodriguez Triple Junction in the Indian Ocean ranged from 1.1 to 1.46, with higher *b*-values reported for the segment axis with higher spreading rates (Katsumata et al. 2001). *b*-values at 23°N in the Mid-Atlantic Ridge (MAR) ranged from 0.75 to 1.2 (Toomey et al. 1988). The *b*-values at 26°N in the MAR also ranged between 0.9 and 2.25 (Kong et al. 1992). Since both *b*-values in the MAR were estimated using seismic moments, the *b*-values obtained from seismic moments were converted to the magnitude

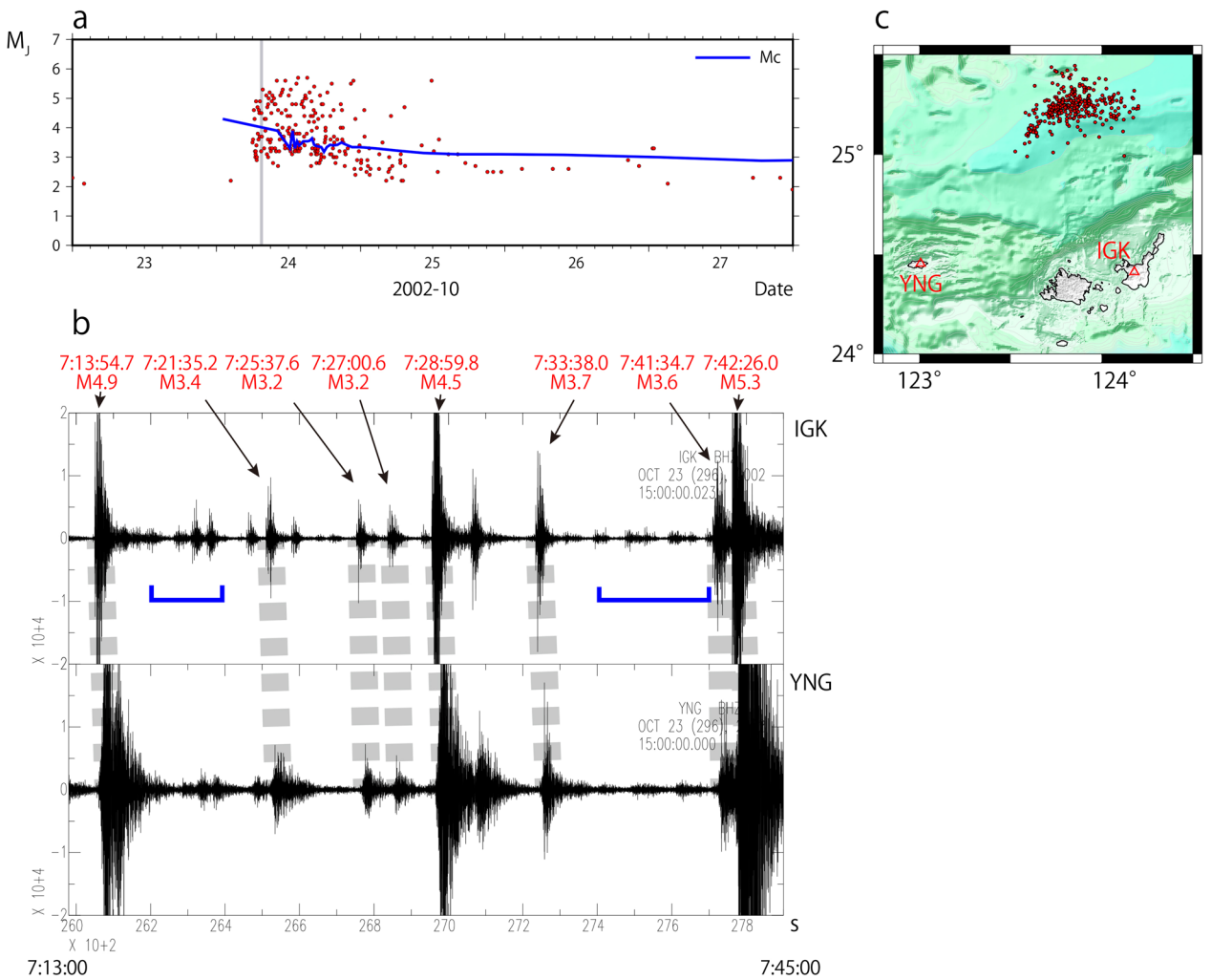

Fig. 5 Time–magnitude diagrams and observed waveforms of the October 2002 earthquake swarm in the eastern YA. **a** Time–magnitude diagram. The broken blue line shows the time variation of M_C. The M_C was calculated by shifting by 5% for every 100 earthquakes. The gray hatch indicates the time range of the waveforms displayed in **b**. **b** Vertical component waveforms at IGK and YNG F-net stations with 1 Hz high-pass filtering, from 7:13:00 to 7:45:00 JST, October 24, 2002. Gray dotted lines indicate the earthquakes with hypocenters determined by the JMA. Blue lines indicate periods in which the waveform at IGK showed multiple spindle-shaped waveforms. **c** Epicenter distribution in October 2002. Red circles indicate epicenters. The red triangles indicate the F-net stations

case to discuss here. Seismic activity at the MOR is often interpreted as magmatic or tectonic (Bohnenstiehl et al. 2008). Higher *b*-values at the MOR are also thought to reflect magmatic activity (Tolstoy et al. 2001) or strong tectonic heterogeneity (Bohnenstiehl et al. 2008). Applying the example at the MOR to the Okinawa Trough, a *b*-value of less than 2.0 at the Okinawa Trough suggests that earthquake swarms at the Okinawa Trough might be strongly tectonically influenced or might be occurring at locations where the structural heterogeneity is not extremely strong.

However, the improvement in the spatio-temporal resolution of seismic activity may reveal the spatio-temporal heterogeneity of *b*-values. In the geothermal area, the *b*-value varies in complex ways. In the Yellowstone volcanic field, *b*-values are normal to high in most areas, with localized low *b*-value regions (Farrell et al. 2009). For the 2008–2009 Yellowstone earthquake swarm, the *b*-value was 1.1 (Glazner and McNutt 2021). This earthquake swarm was interpreted to have been triggered by the movement of magmatic fluid or poroelastic stress pulses (Farrell et al. 2010). In other cases, the 2014 southeastern Long Valley Caldera swarm showed a temporary decrease in *b*-values when the swarm activity (~1 km scale) occurred on faults that reflected the regional stress field, followed by an increase in *b*-values when the swarm

activity occurred on the nearby non-parallel faults (Shelly et al. 2016). The spatial resolution of ~ 10 m and the fact that M_C captures earthquakes as small as -0.4, even very small earthquakes, capture fine-scale statio-temporal *b*-value change. In the Okinawa Trough, if the accuracy of hypocenter determination is improved, it would be possible to distinguish between areas of decreasing *b*-value due to increased stress and areas of high *b*-value due to hydrothermal activity in the swarm seismic activity area. For example, the YO has a higher *b*-value than the other Okinawa Trough rift-axis (Fig. 3a). This area is located on the Daiyon-Yonaguni knoll, where active hydrothermal activity has been reported (Ishibashi et al. 2015). This means that even in the rift-axis of the Okinawa Trough, the *b*-value is higher where hydrothermal activity is active. Since dyke intrusion and hydrothermal activity are occurring in the rift-axis of the Okinawa Trough, these might have resulted in a narrow distribution of low and high *b*-value regions. However, this might not be detectable due to the insufficient accuracy of hypocenter determination. Therefore, it is necessary to develop a seismic observation system on the seafloor in the Okinawa Trough.

Conclusions

The spatial distribution of *b*-values in the central and southern Okinawa troughs shows that *b*-values are not low, in contrast to the previous study. One factor contributing to this was that the previous study did not consider the spatial variation of M_C. The M_C is particularly large in the rift-axis of the Okinawa Trough. In the rift-axis of the Okinawa Trough, the earthquake detection capability was temporarily reduced by a large number of earthquake swarms occurring in a short period, which caused the M_C to increase. In addition, the discrepancy between M_J and M_W values near the Okinawa Trough caused the *b*-value to be underestimated. Since the same equation for $M_J$is used for all of Japan, it might not be easy to use a revised equation only for the Okinawa Trough. However, when evaluating seismic activity in the region of the Okinawa Trough, one should be aware of this property of M_J before using it.

Abbreviations

AM: Amami area; CMT: Centroid moment tensor; F-net: Full Range Seismograph Network of Japan; FMD: Frequency–magnitude distribution; JMA: Japan Meteorological Agency; JST: Japan Standard Time; KU: Kumejima area; MAR: Mid-Atlantic Ridge; M_C: Magnitude completeness; M_d: Displacement magnitude using fewer than three stations; MD: Displacement magnitude; *MI*: Miyako area; M_J: JMA magnitude; MOR: Mid-ocean ridge; M_v: Velocity magnitude using fewer than three stations; M_V: Velocity magnitude; M_W: Moment magnitude; NIED: National Research Institute for Earth Science and Disaster Resilience; YA: Yaeyama area; YO: Yonaguni area.

Supplementary Information

The online version contains supplementary material available at https://doi.org/10.1186/s40623-022-01739-7.

Additional file 1: Table S1. The list of earthquakes that determined the M_v and its M_v.

Additional file 2: Figure S1. Time variation of M_C in the MI. **a** Cumulative number of earthquakes ($M_V \geq 3.0$). The calculation area is shown at Figurer 1a. **b** Time variation of M_C. The M_C was calculated using Zmap7, shifting by 5% for every 100 earthquakes on the time axis. Figure S2. The same as Figure S1 but in the AM. Figure S3. Examples of ill-behaved and well behaved FMD. **a** Ill-behaved FMD. The dashed line indicates the minimum number of earthquakes for which M_C and *b*-values were determined. **b** Well behaved FMD. Figure S4. Distribution of *b*-values and M_C in the south-central part of the Ryukyu determined by M_J. **a** Distribution of *b*-values. The location of the plate boundary is from Bird (2003). **b** Distribution of M_C. Figure S5. Frequency distribution of M_C in each region. **a** Frequency distribution of M_C in the southern Okinawa Trough. M_C values were calculated using M_V. Numbers with arrows show the M_C for the entirety of the box. **b** The same as **a** but in the central Okinawa Trough. **c** The same as **a** but in the southern Ryukyu arc. **d** The same as **a** but in the central Ryukyu arc. **e** The area of each region is shown. The M_C values are shown in color. The location of the plate boundary is from Bird (2003). Figure S6. Distribution of earthquakes color-coded by the number of seismic stations used to determine the hypocenter. **a** Distribution of earthquakes of M3.0–4.0. The color indicates the number of seismic stations used to determine the hypocenter. **b** The same as **a**, but for earthquakes of M2.0–3.0. **c** Distribution of *b*-values. The data are the same as Fig. 3a.

Acknowledgements

I am grateful to the Japan Meteorological Agency for providing the earthquake catalog. I am also grateful for the NIED F-net waveform records and CMT solutions. M_C and *b*-value analysis was performed using ZMAP 7 software (https://github.com/CelsoReyes/zmap7). Generic Mapping Tools (Wessel et al. 2019) was used to create figures. I thank Dr. David Shelly and the anonymous reviewer for providing constructive comments that helped to improve this manuscript.

Author contributions

NM carried out the analyses and drafted the manuscript. The author read and approved the final manuscript.

Funding

This study was partially supported by Association for the Development of Earthquake Prediction and JSPS KAKENHI Grant number 21H01167.

Availability of data and materials

The datasets used in this study are available from MN upon reasonable request.

Declarations

Ethics approval and consent to participate

Not applicable.

Consent for publication

Not applicable.

Competing interests

The author declares that they have no competing interests.

Received: 23 August 2022 Accepted: 8 November 2022
Published online: 02 December 2022

References

Aki K (1965) Maximum likelihood estimate of b in the formula log N=a-bM and its confidence limits. Bull Earthq Res Inst Univ Tokyo 43:237–239. https://repository.dl.itc.u-tokyo.ac.jp/record/33631/files/ji0432001.pdf

Arai R (2021) Characteristics of seismicity in the southern Okinawa Trough and their relation to back-arc rifting processes. Earth Planets Space 73:160. https://doi.org/10.1186/s40623-021-01491-4

Arai R, Kodaira S, Yuka K, Takahashi T, Miura S, Kaneda Y (2017) Crustal structure of the southern Okinawa Trough: Symmetrical rifting, submarine volcano, and potential mantle accretion in the continental back-arc basin. J Geophys Res Solid Earth 122:622–641. https://doi.org/10.1002/2016JB013448

Bird P (2003) An updated digital model of plate boundaries. Geochem Geophys Geosyst 4:1027. https://doi.org/10.1029/2001GC000252

Bohnenstiehl DR, Waldhauser F, Tolstoy M (2008) Frequency-magnitude distribution of microearthquakes beneath the 9°50′N region of the East Pacific Rise, October 2003 through April 2004. Geochem Geophys Geosyst 9:1003. https://doi.org/10.1029/2008GC002128

Chikasada N (2020) Global tsunami terrain model. Accessed Jun 22, 2022. https://doi.org/10.17598/NIED.0021

Data Analysis Section, Earthquake Prediction Information Division, Seismological and Volcanological Department, Japan Meteorological Agency (2004) A study on the comparison of the new JMA magnitude with other magnitudes. Quart J Seismol JMA 67:21–35. https://www.jma.go.jp/jma/kishou/books/kenshin/vol67p021.pdf (**in Japanese with English abst.**)

Farrell J, Husen S, Smith RB (2009) Earthquake swarm and b-value characterization of the Yellowstone volcano-tectonic system. J Volcanol Geotherm Res 188:260–276. https://doi.org/10.1016/j.jvolgeores.2009.08.008

Farrell J, Smith RB, Taira T, Chang WL, Puskas CM (2010) Dynamics and rapid migration of the energetic 2008–2009 Yellowstone Lake earthquake swarm. Geophys Res Lett 37:L19305. https://doi.org/10.1029/2010GL044605

Funasaki J, Earthquake Prediction Information Division (2004) Revision of the JMA velocity magnitude. Quart J Seismol JMA 67:11–20. https://www.jma.go.jp/jma/kishou/books/kenshin/vol67p011.pdf (**in Japanese with English abst.**)

Glazner AF, McNutt SR (2021) Relationship between dike injection and *b*-value for volcanic earthquake swarms. J Geophys Res Solid Earth 126:e2020JB021631. https://doi.org/10.1029/2020JB021631

Gutenberg B, Richter CF (1944) Frequency of earthquakes in California. Bull Seismol Soc Am 34:185–188. https://doi.org/10.1785/BSSA0340040185

Ishibashi J, Ikegami F, Tsuji T, Urabe T (2015) Hydrothermal activity in the Okinawa Trough back-arc basin: Geological background and hydrothermal mineralization. In: Ishibashi J, Okino K, Sunamura M (eds) Subseafloor biosphere linked to hydrothermal systems. Springer, Tokyo, pp.337–359. https://doi.org/10.1007/978-4-431-54865-2

Kagan YY (2004) Short-term properties of earthquake catalogs and models of earthquake source. Bull Seismol Soc Am 94:1207–1228. https://doi.org/10.1785/012003098

Kanbayashi Y, Ichikawa M (1977) A method for determining magnitude of shallow earthquake occurring in and near Japan. Quart J Seismol JMA 41:57–61. https://www.jma.go.jp/jma/kishou/books/kenshin/vol41p057.pdf (**in Japanese with English abst.**)

Katsumata A (2004) Revision of the JMA displacement magnitude. Quart J Seismol JMA 67:1–10. https://www.jma.go.jp/jma/kishou/books/kenshin/vol67p001.pdf (**in Japanese with English abst.**)

Katsumata A (2007) Magnitude determination of deep-focus earthquakes in and around Japan with regional velocity-amplitude data (II). Pap Met Geophys 58:31–61. https://doi.org/10.2467/mripapers.58.31

Katsumata M (1964) A method to determine the magnitude of deep-focus earthquakes in and near Japan. Zisin 2(17):158–165. https://doi.org/10.4294/zisin1948.17.3_158 (**in Japanese with English abst.**)

Katsumata K, Sato T, Kasahara J, Hirata N, Hino R, Takahashi N, Sekine M, Miura S, Koresawa S, Wada N (2001) Microearthquake seismicity and focal mechanisms at the Rodriguez Triple Junction in the Indian Ocean using ocean bottom seismometers. J Geophys Res 106(12):30689–30699. https://doi.org/10.1029/2000JB000106

Kong LSL, Solomon SC, Purdy GM (1992) Microearthquake characteristics of a Mid-Ocean Ridge along-axis high. J Geophys Res 97:1659–1685. https://doi.org/10.1029/91JB02566

Nakamura M, Kinjo A (2018) Activated seismicity by strain rate change in the Yaeyama region, south Ryukyu. Earth Planets Space 70:154. https://doi.org/10.1186/s40623-018-0929-y

Nanjo KZ, Hirata N, Obara K, Kasahara K (2012) Decade-scale decrease in *b* value prior to the M9-class 2011 Tohoku and 2004 Sumatra quakes. Geophys Res Lett 39:L20304. https://doi.org/10.1029/2012GL052997

Ogata Y (1983) Estimation of the parameters in the modified Omori formula for aftershock frequencies by the maximum likelihood procedure. J Phys Earth 31:115–124. https://doi.org/10.4294/jpe1952.31.115

Scholz CH (1968) The frequency–magnitude relation of microfracturing in rock and its relation to earthquakes. Bull Seismol Soc Am 58:399–415. https://doi.org/10.1785/BSSA0580010399

Schorlemmer D, Wiemer S (2005) Microseismicity data forecast rupture area. Nature 434:1086. https://doi.org/10.1038/4341086a

Shelly DR, Ellsworth WL, Hill DP (2016) Fluid-faulting evolution in high definition: connecting fault structure and frequency-magnitude variations during the 2014 Long Valley Caldera California, Earthquake Swarm. J Geophys Res Solid Earth 121:1776–1795. https://doi.org/10.1002/2015JB012719

Takeuchi H (1983) Magnitude determination of small shallow earthquake with JMA electromagnetic seismograph model 76. Quart J Seismol JMA 47:112–116. https://www.jma.go.jp/jma/kishou/books/kenshin/vol47p112.pdf (**in Japanese with English abst.**)

Toomey DR, Solomon SC, Purdy GM (1988) Microearthquakes beneath Median Valley of Mid-Atlantic Ridge near 23°N: Tomography and tectonics. J Geophys Res 93:9093–9112. https://doi.org/10.1029/JB093iB08p09093

Tolstoy M, Bohnenstiehl DR, Edwards MH, Kurras GJ (2001) Seismic character of volcanic activity at the ultraslow-spreading Gakkel Ridge. Geology 29:1139–1142. https://doi.org/10.1130/0091-7613(2001)029%3c1139:SCOVAA%3e2.0.CO;2

Tsuboi C (1954) Determination of the GUTENBERG-RICHTER'S Magnitude of Earthquakes occurring in and near Japan. Zisin 2(7):185–193. https://doi.org/10.4294/zisin1948.7.3_185 (**in Japanese with English abst.**)

Tu Y, Heki K (2017) Decadal modulation of repeating slow slip event activity in the southwestern Ryukyu arc possibly driven by rifting episodes at the Okinawa Trough. Geophys Res Lett 44:9308–9313. https://doi.org/10.1002/2017GL074455

Utsu T (1965) A method for determining the value of *b* in a formula log $n = a - bM$ showing the magnitude-frequency relation for earthquakes. Geophys Bull Hokkaido Univ 13:99–103. https://eprints.lib.hokudai.ac.jp/dspace/bitstream/2115/13887/1/13_p99-103.pdf (**in Japanese with English abst.**)

Utsu T (1971) Aftershocks and earthquakes statistics (III): Analysis of the distribution of earthquakes in magnitude, time and space with special considerations to clustering characteristics of earthquakes occurrence (1). J Fac Sci Hokkaido Univ Series VII 3:379–441

Utsu T, Ogata Y, Matsuura RS (1995) The centenary of the Omori formula for a decay law of aftershock activity. J Phys Earth 43:1–33. https://doi.org/10.4294/jpe1952.43.1

Wessel P, Luis JF, Uieda L, Scharroo R, Wobbe F, Smith WHF, Tian D (2019) The Generic Mapping Tools version 6. Geochem Geophys Geosyst 20:5556–5564. https://doi.org/10.1029/2019GC008515

Wiemer S (2001) A software package to analyze seismicity: ZMAP. Seismol Res Lett 72:373–382. https://doi.org/10.1785/gssrl.72.3.373

Wiemer S, Katsumata K (1999) Spatial variability of seismicity parameters in aftershock zones. J Geophys Res 104:13135–13151. https://doi.org/10.1029/1999JB900032

Wiemer S, Wyss M (1997) Mapping the frequency-magnitude distribution in asperities: an improved technique to calculate recurrence times? J Geophys Res 102:15115–15128. https://doi.org/10.1029/97JB00726

Wiemer S, Wyss M (2000) Minimum Magnitude of Completeness in Earthquake Catalogs: Examples from Alaska, the Western United States, and Japan. Bull Seismol Soc Am 90:859–869. https://doi.org/10.1785/011999090114

Wiemer S, Wyss M (2002) Mapping spatial variability of the frequency magnitude distribution of earthquakes. Adv Geophys 45:259–302. https://doi.org/10.1016/S0065-2687(02)80007-3

Publisher's Note